

Contact Resistance and Megahertz Operation of Aggressively Scaled Organic Transistors

Frederik Ante, Daniel Kälblein, Tarek Zaki, Ute Zschieschang, Kazuo Takimiya, Masaaki Ikeda, Tsuyoshi Sekitani, Takao Someya, Joachim N. Burghartz, Klaus Kern, and Hagen Klauk*

Organic thin-film transistors (TFTs) are of interest for large-area electronics applications, such as conformable sensor arrays and flexible active-matrix displays, in which the TFTs will typically operate at frequencies below about 100 kHz.^[1–5] For more demanding applications, such as high-resolution video displays with integrated row and column drivers, TFTs capable of operating at frequencies up to about 10 MHz will be required. The cutoff frequency f_T of a field-effect transistor is often calculated using Equation (1):^[6]

$$f_T \approx \frac{\mu_{\text{eff}} (V_{\text{GS}} - V_{\text{th}})}{2\pi L(L + 2L_C)} \quad (1)$$

with the effective charge-carrier mobility μ_{eff} , the gate–source voltage V_{GS} , the threshold voltage V_{th} , the channel length L , and the contact length L_C . The contact length L_C is the distance by which the gate electrode overlaps the source and drain contacts (see **Figure 1a**). The reason why L_C appears in Equation (1) is that this overlap creates a parasitic capacitance that is charged and discharged during each switching event. Intuitively, the contact length L_C should therefore be minimized to achieve the highest possible cutoff frequency.^[7,8]

Equation (1) suggests that for an effective mobility of $1 \text{ cm}^2 (\text{V s})^{-1}$ and lateral dimensions (L , L_C) of $1 \mu\text{m}$, a cutoff frequency of 10 MHz can be achieved at a voltage of 3 V (or a frequency of 100 MHz at 30 V). Effective mobilities around $1 \text{ cm}^2 (\text{V s})^{-1}$ are indeed commonly measured in organic

TFTs, but usually only if the channel length is much larger than $1 \mu\text{m}$.^[9–11] When the channel length is reduced to about $1 \mu\text{m}$, the channel resistance R_{channel} becomes smaller than the contact resistance R_C , thus causing the effective mobility μ_{eff} of the transistor to drop substantially below the intrinsic mobility μ_0 of the semiconductor:^[12,13]

$$\mu_{\text{eff}} \approx \mu_0 \left(1 - \left(\frac{\mu_0 C_i W R_C (V_{\text{GS}} - V_{\text{th}})}{L + \mu_0 C_i W R_C (V_{\text{GS}} - V_{\text{th}})} \right)^2 \right) \quad (2)$$

with the gate-dielectric capacitance per unit area C_i and the channel width W . This is why the effective mobility μ_{eff} in TFTs with aggressively reduced dimensions is usually below $1 \text{ cm}^2 (\text{V s})^{-1}$, even if the semiconductor is known to have a much larger intrinsic mobility μ_0 . This is also why cutoff frequencies reported for organic TFTs rarely exceed 1 MHz.^[7,8,14,15] A record cutoff frequency of 28 MHz measured at a relatively high voltage of 25 V has been reported for TFTs based on the fullerene C_{60} having a channel length of $2 \mu\text{m}$.^[16] TFTs based on C_{60} as the semiconductor can have large effective mobilities ($2.2 \text{ cm}^2 (\text{V s})^{-1}$ in Reference [16]), but they cannot be operated in air.

The above-mentioned influence of the channel length on the effective mobility and on the cutoff frequency of organic TFTs has been studied in great detail.^[12] Most of these studies employed TFTs with the coplanar structure, since in this architecture the source and drain contacts are fabricated prior to the deposition of the organic semiconductor layer and thus can be patterned with high resolution

Dr. F. Ante, Dr. D. Kälblein, Dr. U. Zschieschang, Prof. K. Kern,
 Dr. H. Klauk
 Max Planck Institute for Solid State Research
 Heisenbergstr. 1, 70569 Stuttgart, Germany
 E-mail: H.Klauk@fkf.mpg.de

T. Zaki, Prof. J. N. Burghartz
 Institut für Mikroelektronik/IMS CHIPS
 Allmandring 30a, 70569 Stuttgart, Germany

Prof. K. Takimiya
 Department of Applied Chemistry
 Graduate School of Engineering
 Institute for Advanced Materials Research
 Hiroshima University
 Higashi-Hiroshima, Japan

DOI: 10.1002/sml.201101677

Dr. M. Ikeda
 Functional Chemicals R&D Laboratories
 Nippon Kayaku Co., Ltd.,
 Kita-ku, Tokyo, Japan

Prof. T. Sekitani, Prof. T. Someya
 Department of Electrical Engineering
 University of Tokyo
 Tokyo, Japan

Prof. K. Kern
 Institut de Physique de la Matière Condensée
 École Polytechnique Fédérale de Lausanne
 1015 Lausanne, Switzerland



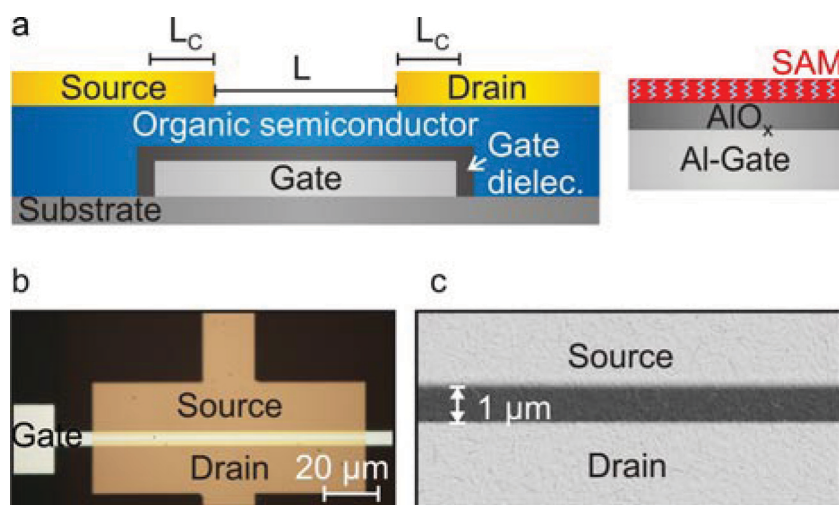


Figure 1. a) Schematic cross section illustrating the inverted staggered (bottom-gate, top-contact) organic TFT structure. The extent of the channel length L and of the contact length L_C as well as the structure of the gate dielectric are indicated. b) Photograph showing a dinaphtho[2,3-*b*:2',3'-*f*]thieno[3,2-*b*]thiophene (DNNT) TFT with a channel length of 1 μm and a contact length of 2 μm manufactured using silicon stencil masks. c) Scanning electron microscopy (SEM) image depicting the well-defined channel length of 1 μm and the smooth contact edges. SAM = self-assembled monolayer.

by photolithography or electron-beam lithography. However, experiments^[12] and simulations^[17] show that coplanar organic TFTs often have a large contact resistance, since the gate field is partially shielded by the source and drain contacts and a channel is thus induced only in the region between the contacts. As a result, in coplanar organic TFTs the efficient charge transfer between the contacts and the semiconductor is limited to the narrow regions where the gate-induced channel touches the contact edges.^[17] In staggered TFTs the source and drain contacts are located opposite the gate dielectric, so the channel extends beyond the contact edges along the entire contact length L_C . As a result, in staggered TFTs the area available for charge transfer is much larger than in coplanar TFTs,^[17] which explains why staggered organic TFTs often have a smaller contact resistance than coplanar organic TFTs.^[12]

An important question arising from these considerations is to what extent the contact length L_C affects the contact resistance R_C in staggered organic TFTs. In all previous studies on the contact resistance of staggered organic TFTs the contact length L_C was very large (tens of micrometers), so that the influence of L_C on R_C was insignificant.^[12,18,19] The fact that the contact resistance and the effective mobility of staggered TFTs are indeed affected when the contact length L_C is reduced is already known from transistors based on amorphous silicon,^[20] microcrystalline silicon,^[21] carbon nanotubes,^[22] silicon nanowires,^[23] and graphene.^[24]

Herein, we provide a rigorous analysis of the complex relationships between contact length, contact resistance, and effective mobility in aggressively scaled staggered organic TFTs. We also show that achieving a high cutoff frequency in staggered organic TFTs is not as simple as minimizing L and L_C , as Equation (1) would suggest. For this study we fabricated staggered (bottom-gate, top-contact) TFTs based on the air-stable organic semiconductor dinaphtho[2,3-*b*:2',3'-*f*]

thieno[3,2-*b*]thiophene (DNNT) with channel lengths L ranging from 60 to 1 μm and well-defined contact lengths L_C of 200, 20, 5, and 2 μm . To realize top-contact organic TFTs with such small dimensions without exposing the semiconductor layer to potentially harmful organic solvents during photolithography or electron-beam lithography,^[25] we took advantage of high-resolution silicon stencil masks (see Figure S1, Supporting Information).^[26–30]

To fabricate fully patterned TFTs, a set of four stencil masks is required. The first mask is used to define the gate electrodes, which consist of 30-nm-thick aluminum deposited by thermal evaporation in vacuum. With the second mask, small areas on the aluminum required for electrical probing are covered with 20-nm-thick gold to prevent the formation of an insulating layer in these areas. The gate dielectric is a combination of 3.6-nm-thick plasma-grown AlO_x and a 1.7-nm-thick tetradecylphosphonic acid self-assembled

monolayer (SAM) and has a capacitance per unit area (C_i) of 800 nF cm^{-2} .^[31] Through the third stencil mask a 25-nm-thick layer of the organic semiconductor DNNT is deposited by sublimation in vacuum.^[9,31,32] Finally, 25-nm-thick gold source and drain contacts are deposited by thermal evaporation through the fourth stencil mask. The schematic cross section and a photograph of a completed transistor with a channel length of 1 μm and a contact length of 2 μm are shown in Figure 1b. The SEM image in Figure 1c depicts the sharp contact edges of a TFT with a channel length of 1 μm . The atomic force microscopy (AFM) image in Figure S2 highlights the well-defined overlaps between the gate electrode and the source and drain contacts that can be achieved by stencil-mask patterning. All electrical measurements were performed in ambient air at room temperature.

The electrical characteristics of a DNNT TFT with a large channel length ($L = 60 \mu\text{m}$) and large contact length ($L_C = 200 \mu\text{m}$) are shown in **Figure 2**. From the transfer characteristics of this DNNT TFT, an effective mobility of $2.4 \text{ cm}^2 (\text{V s})^{-1}$ is extracted in both the saturation and the linear region. This effective mobility is close to the intrinsic mobility of $3 \text{ cm}^2 (\text{V s})^{-1}$ which we have calculated by applying the transmission line method (TLM)^[12,32] to a set of DNNT TFTs with channel lengths ranging from 60 to 1 μm and a contact length of 200 μm . The TLM analysis also indicates that these TFTs have a relatively small width-normalized contact resistance of 0.6 $\text{k}\Omega \text{ cm}$ (see Figure S3).

When the channel length is reduced, the relative contribution of the contact resistance to the total device resistance increases and, thus, the effective mobility decreases. For example, the DNNT TFT in Figure S4, which has a small channel length (1 μm) and a large contact length (200 μm), has an effective mobility that is notably smaller than the intrinsic mobility ($0.4 \text{ cm}^2 (\text{V s})^{-1}$ in the saturation region, $0.2 \text{ cm}^2 (\text{V s})^{-1}$ in the linear region). The effective mobilities

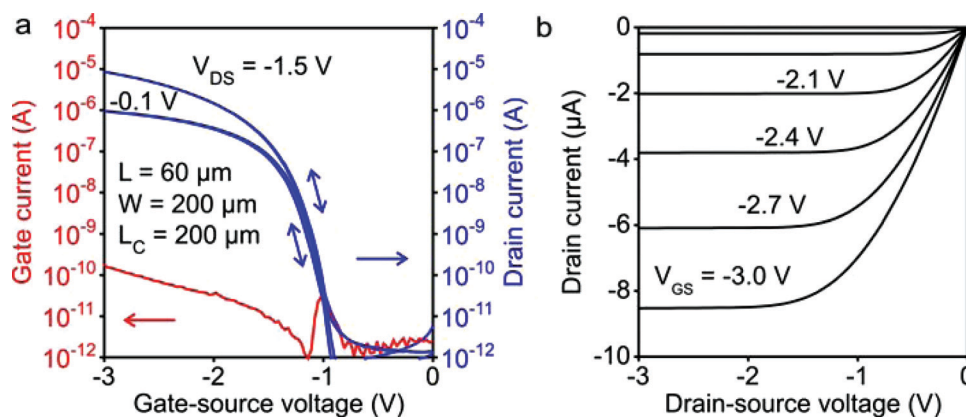


Figure 2. Transfer and output characteristics of a DNTT TFT with relaxed dimensions. The transistor has a channel length of 60 μm and a contact length of 200 μm . From the transfer characteristics, effective mobilities of 2.4 $\text{cm}^2 (\text{V s})^{-1}$ (both in the saturation region and in the linear region), an on/off current ratio of 10^6 , a subthreshold swing of 100 mV decade $^{-1}$, and a threshold voltage of -1.4 V are extracted.

of a set of DNTT TFTs with channel lengths ranging from 60 to 1 μm and a contact length of 200 μm are summarized in Figure S5. As can be seen, both the saturation mobility and the linear mobility decrease significantly with decreasing channel length. This effect is somewhat less pronounced in the saturation region than in the linear region, presumably because the contribution of the contact resistance to the total device resistance is somewhat smaller when the channel near the drain contact is pinched off.^[33] The excellent parameter uniformity of DNTT TFTs with channel lengths between 1 and 5 μm fabricated using high-resolution silicon stencil masks is demonstrated in **Figure 3**.

From the TLM analysis in Figure S3 we can also extract the transfer length L_T , which is the characteristic length over which 63% of the charge-carrier exchange between the contacts and the semiconductor occurs.^[34] For our DNTT TFTs this transfer length is 10 μm , which is in good agreement with previous reports on the transfer length in organic TFTs.^[12,18,19,30,35] **Figure 4** shows that the output characteristics of the DNTT TFTs change dramatically when the contact length L_C is reduced from a value much larger than the transfer length L_T (Figure 4a; $L_C = 200 \mu\text{m}$) to a value similar to or smaller than the transfer length L_T (Figure 4b–d; $L_C = 20, 5, 2 \mu\text{m}$). As can be seen, the undesirable nonlinearity of the drain current at small drain-source voltages becomes

more and more pronounced as the contact length L_C is reduced below the transfer length L_T . At the same time, the effective mobility (both in the saturation region and in the linear region) decreases with decreasing contact length (see Figure 4e). These observations indicate that reducing the contact length L_C below the transfer length L_T causes the contact resistance to increase considerably.

To analyze the relationship between the transfer length, the contact length, and the contact resistance, we applied the TLM method to sets of DNTT TFTs with contact lengths of 200, 20, 5, and 2 μm (see Figure S6). The extracted contact resistances are 0.6, 0.7, 1.4, and 2.2 $\text{k}\Omega \text{ cm}$, respectively (see Figure 4f). Also included in Figure 4f is the contact resistance of 9.8 $\text{k}\Omega \text{ cm}$ which we have recently measured for a staggered DNTT TFT with a contact length of 0.2 μm fabricated by electron-beam lithography,^[32] as well as the theoretically expected relation between the contact resistance R_C and the contact length L_C given by:^[34]

$$R_C \cdot W = 2 \cdot R_{\text{sheet}} L_T \coth\left(\frac{L_C}{L_T}\right) \quad (3)$$

where R_{sheet} is the sheet resistance of the semiconductor layer. The black curve in Figure 4f is calculated with Equation (3) using the sheet resistance and the transfer length extracted

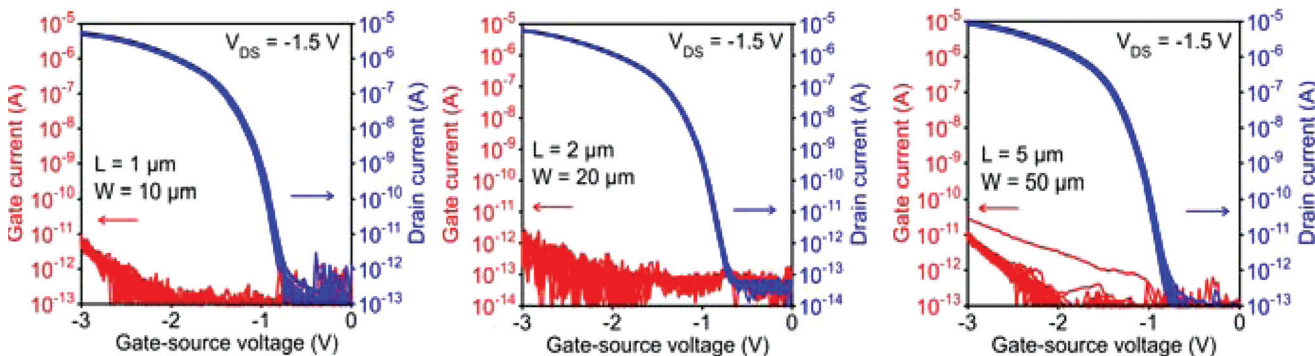


Figure 3. Transfer characteristics of 47 DNTT TFTs with channel lengths of 1 μm (left; 16 TFTs), 2 μm (center; 15 TFTs), and 5 μm (right; 16 TFTs). All TFTs have a contact length of 20 μm .

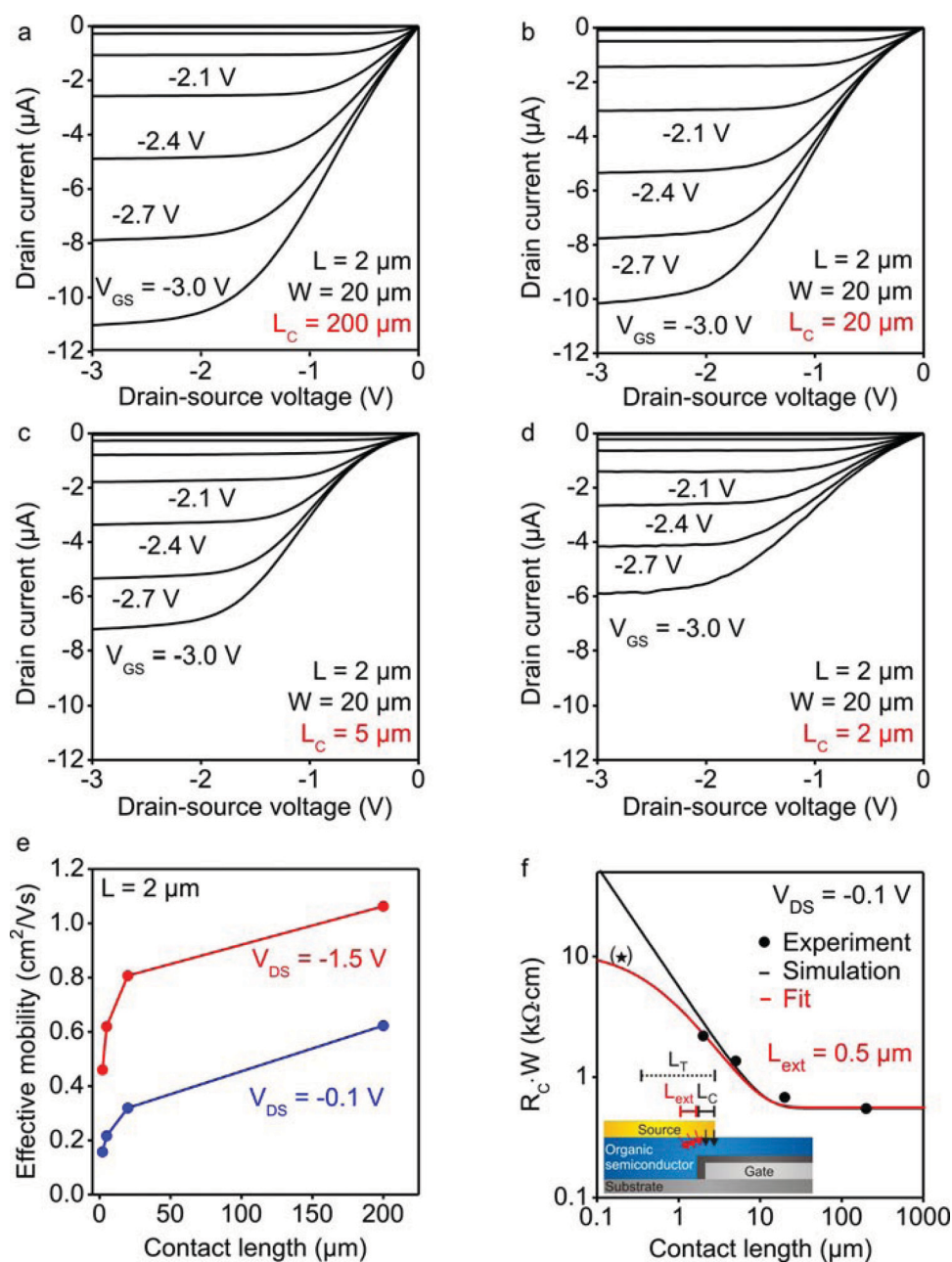


Figure 4. Electrical characteristics of DNTT TFTs for different contact lengths. a–d) Output characteristics of DNTT TFTs with a channel length of 2 μm and contact lengths of 200, 20, 5, and 2 μm . When the contact length is large ($L_c = 200 \mu\text{m}$; (a)), the relation between the drain current and the drain–source voltage at small drain–source voltages is almost linear. When the contact length is reduced close to or below the value of the transfer length (b–d), the undesirable nonlinearity of the drain current becomes more pronounced. e) Effective mobilities of DNTT TFTs with a channel length of 2 μm as a function of the contact length in the saturation region (red curve) and in the linear region (blue curve). The effective mobilities in both the saturation and the linear region decrease with decreasing contact length, thereby indicating a systematic increase of the contact resistance. f) Width-normalized contact resistance as a function of the contact length. The data points indicate contact resistances of 0.6, 0.7, 1.4, and 2.2 $\text{k}\Omega \text{ cm}$ measured for contact lengths of 200, 20, 5, and 2 μm , respectively. The black curve describes the theoretically expected relation between the contact resistance and the contact length given by Equation (3), while the red curve is a fit to Equation (4) that takes into account the contribution of the extended contact length L_{ext} . Note that the contact resistance of 9.8 $\text{k}\Omega \text{ cm}$ for a contact length of 0.2 μm was not included in the fitting procedure, since this transistor was fabricated with a different technology.^[32] The inset illustrates the concept of the extended contact length that leads to a larger active contact region.

from the TLM analysis summarized in Figure S3 ($R_{sheet} = 270 \text{ k}\Omega \text{ sq}^{-1}$, $L_T = 10 \mu\text{m}$). For long contact lengths ($L_c \geq 20 \mu\text{m}$) the agreement between the measurement data and the calculated curve is reasonably good. However, for short

contact lengths ($L_c \leq 5 \mu\text{m}$) the measured contact resistance is notably smaller than predicted by Equation (3). The reason is that Equation (3) only takes into account the charge transfer between the contacts and the semiconductor channel in

the direction perpendicular to the surface of the gate electrode (black arrows in the inset of Figure 4f). However, two-dimensional numerical simulations^[36] suggest that the electrostatic potential distribution in the organic semiconductor leads to an additional contribution to the charge transfer between the contacts and the channel in a nonperpendicular direction (red arrows in the inset of Figure 4f) and thus to an additional contribution to the contact length L_C . By taking into account this additional contribution, that is, the extended contact length L_{ext} , Equation (3) can be rewritten as follows:

$$R_C \cdot W = 2 \cdot R_{\text{sheet}} L_T \coth \left(\frac{L_C + L_{\text{ext}}}{L_T} \right) \quad (4)$$

By fitting the measured contact resistances with Equation (4), we obtain $L_{\text{ext}} = 0.5 \mu\text{m}$ (see red curve in Figure 4f). Note that the contact resistance of $9.8 \text{ k}\Omega \text{ cm}$ for a contact length of $0.2 \mu\text{m}$ was not included in the fitting procedure, since this transistor was fabricated with a different technology (using electron-beam lithography, rather than stencil masks).

Despite this extension of the contact length, a reduction of the contact length below the transfer length leads to a noticeable increase in the contact resistance R_C and hence to a significant reduction in the effective mobility μ_{eff} . This contact-length dependence of the effective mobility has a pronounced effect on the cutoff frequency of the transistors. To illustrate this effect we calculated the cutoff frequency expected for a staggered organic TFT with an intrinsic mobility of $3 \text{ cm}^2 (\text{V s})^{-1}$ as a function of the channel length L and the contact length L_C using Equations (1) and (2) and making four different, more or less realistic assumptions for the contact resistance R_C (see **Figure 5**). Under the assumption that the contact resistance is zero, the cutoff frequency increases strongly and monotonically with decreasing contact length and channel length, eventually exceeding 1 GHz for lateral dimensions below 100 nm ($R_C = 0 \text{ k}\Omega \text{ cm}$, see Figure 5a). Assuming that the contact resistance is greater than zero, but independent of the contact length, the cutoff frequency still increases monotonically, but less strongly ($R_C = 0.6 \text{ k}\Omega \text{ cm}$, see Figure 5b). Assuming that the contact resistance increases with decreasing contact length as given by Equation (3) ($L_{\text{ext}} = 0 \mu\text{m}$), the cutoff frequency reaches a maximum when the contact length is approximately equal to the transfer length. However, the cutoff frequency decreases sharply as the contact length is reduced significantly below the transfer length ($R_C = R_C(L_C)$, see Figure 5c). Finally, we have taken into account the extended transfer length L_{ext} in the calculation of the cutoff frequency. In this case, the influence of L_{ext} on the contact resistance R_C was accounted for by using Equation (4), and the effect of L_{ext} on the parasitic overlap capacitance was taken into consideration by replacing Equation (1) with Equation (5):

$$f_T \approx \frac{\mu_{\text{eff}} (V_{\text{GS}} - V_{\text{th}})}{2\pi L(L + 2(L_C + L_{\text{ext}}))} \quad (5)$$

Figure 5d shows that in this case the cutoff frequency reaches a plateau for a contact length close to the transfer length and then remains approximately constant when the

contact length is reduced further. Note that this surprising result is not immediately apparent from Equation (5) alone. As a result of the limiting effect of the transfer length, the maximum cutoff frequency in this most realistic case is only slightly above 1 MHz (see Figure 5d). As can be seen, achieving a high cutoff frequency in staggered organic TFTs may not necessarily require a reduction of the contact length as close to zero as possible. Rather, a careful analysis of the transfer length of a particular material system may eliminate the often difficult compromise between process robustness and device performance. Also note that for the simulations pictured in Figure 5c and d, the transfer length L_T was taken as equal to $5.5 \mu\text{m}$, which is the value calculated from TLM analysis for the most negative drain–source voltage (-1.5 V) that can be applied to our TFTs without causing the channel to pinch off (see Figure S7).

To measure the dynamic performance of our stencil-mask-patterned DNNT TFTs, we fabricated and characterized 11-stage unipolar ring oscillators on glass substrates. The circuit schematic is shown in Figure S8. A photograph and a measured output signal are shown in **Figure 6a**. In Figure 6b the signal propagation delay per stage extracted from the measured output signals is plotted as a function of the supply voltage for two ring oscillators based on TFTs with different channel length and contact length. For the ring oscillators with $L = 4 \mu\text{m}$ and $L_C = 20 \mu\text{m}$ (blue curve in Figure 6b), the simulation in Figure 5d predicts a cutoff frequency for the TFTs of 200 kHz at a drain–source voltage of 4 V . Our ring oscillator measurements show a minimum signal delay per stage of $6 \mu\text{s}$, which corresponds to a cutoff frequency of 80 kHz ($f_T = 1/2\tau$). The more aggressively scaled ring oscillator employs TFTs with $L = 1 \mu\text{m}$ and $L_C = 5 \mu\text{m}$ (red curve in Figure 6b) and oscillates with a minimum signal delay per stage of 230 ns at a supply voltage of 4.2 V . For these dimensions the simulation in Figure 5d predicts a cutoff frequency for the DNNT TFTs of 0.8 MHz , while the measured signal delay (230 ns) corresponds to a cutoff frequency of 2.2 MHz . As can be seen, the measurement data and the simulation results in Figure 5d agree to within a factor of about two or three. Note that the signal delay per stage is below $1 \mu\text{s}$ even for a supply voltage of 1.2 V .

The IMEC group has reported record signal propagation delays for organic ring oscillators of 190 ns for a supply voltage of 13 V and 400 ns for a supply voltage of 10 V .^[15,37] These circuits are based on pentacene TFTs fabricated on flexible polymeric substrates in the coplanar (bottom-gate, bottom-contact) device structure with lateral dimensions (L , L_C) of $2 \mu\text{m}$. The shortest stage delay of our ring oscillators (230 ns) is within 20% of that reported by the IMEC group (190 ns), despite the smaller supply voltages. For supply voltages below 10 V , the organic ring oscillators demonstrated in this work are to our knowledge the fastest reported so far.

One strategy to increase the cutoff frequency of staggered TFTs beyond the few megahertz demonstrated here is to reduce the transfer length L_T , since this will allow the contact length L_C (and hence the overlap capacitance) to

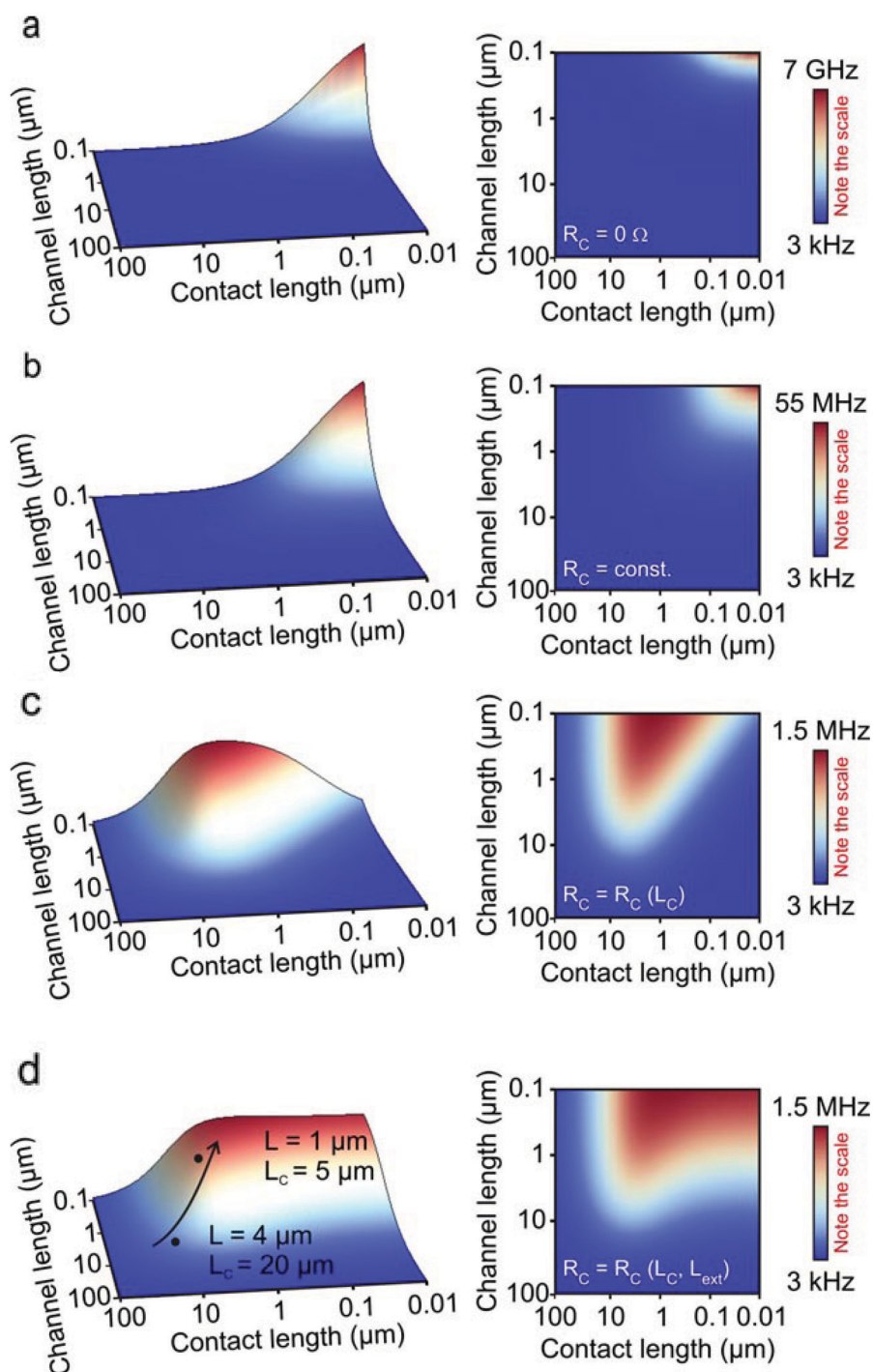


Figure 5. Simulated relation between the channel length, contact length, and cutoff frequency of staggered TFTs using four different assumptions for the contact resistance. a) Assumption 1: The contact resistance is zero. b) Assumption 2: The contact resistance is greater than zero ($0.6 \text{ k}\Omega \text{ cm}$) and independent of the contact length. c) Assumption 3: The contact resistance depends on the contact length as given by Equation (3): $L_{\text{ext}} = 0 \text{ }\mu\text{m}$. d) Assumption 4: The contact resistance depends on the contact length as given by Equation (4): $L_{\text{ext}} = 0.5 \text{ }\mu\text{m}$. For all four simulations, the gate overdrive voltage ($V_{\text{GS}} - V_{\text{th}}$) was set to -1.6 V and the drain–source voltage (V_{DS}) to -4 V .

also be reduced without increasing the contact resistance. For example, for a transfer length of $1 \text{ }\mu\text{m}$, a contact length of $1 \text{ }\mu\text{m}$, and a channel length of $1 \text{ }\mu\text{m}$ our simulations predict a cutoff frequency of 10 MHz . A promising approach to reduce

the transfer length of staggered organic TFTs is area-selective contact doping with a strong organic dopant,^[32] and contact lengths as small as $1 \text{ }\mu\text{m}$ (and below) can be achieved with self-alignment techniques.^[8]

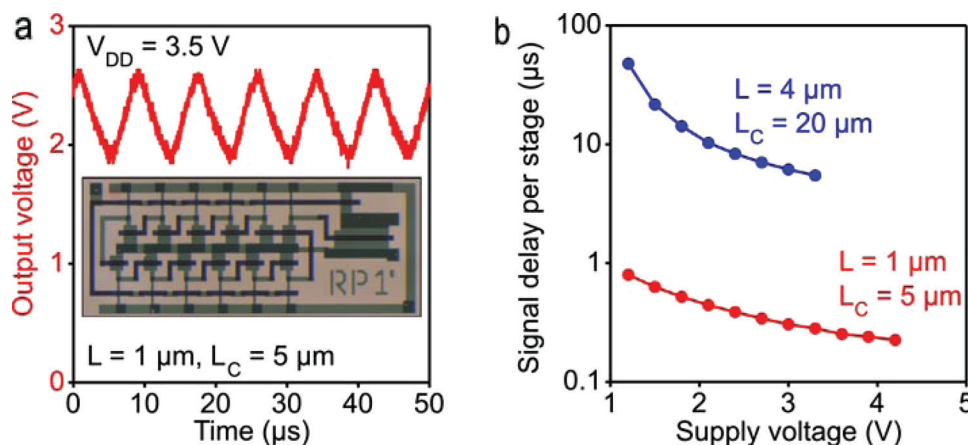


Figure 6. Unipolar ring oscillators based on DNTT TFTs. a) Output signal of a ring oscillator based on DNTT TFTs with a channel length of $1 \mu\text{m}$ and a contact length of $5 \mu\text{m}$ measured at a supply voltage of 3.5 V. The inset shows a photograph of the ring oscillator. b) Signal propagation delay per stage as a function of the supply voltage for 11-stage ring oscillators based on DNTT TFTs having a channel length of $4 \mu\text{m}$ and a contact length of $20 \mu\text{m}$, and on TFTs having a channel length of $1 \mu\text{m}$ and a contact length of $5 \mu\text{m}$. For the latter, a minimum signal delay of 230 ns per stage was measured at a supply voltage of 4.2 V.

Supporting Information

Supporting Information is available from the Wiley Online Library or from the author.

- [1] T. Someya, T. Sekitani, S. Iba, Y. Kato, H. Kawaguchi, T. Sakurai, *Proc. Natl. Acad. Sci. USA* **2004**, *101*, 9966.
- [2] S. Mannsfeld, B. Tee, R. Stoltenberg, C. Chen, S. Barman, B. Muir, A. Sokolov, C. Reese, Z. Bao, *Nat. Mater.* **2010**, *9*, 859.
- [3] I. Yagi, N. Hirai, Y. Miyamoto, M. Noda, A. Imaoka, N. Yoneya, K. Nomoto, J. Kasahara, A. Yumoto, T. Urabe, *J. Soc. Inf. Display* **2008**, *16*, 15.
- [4] G. H. Gelinck, H. E. A. Huitema, E. van Veenendaal, E. Cantatore, L. Schrijnemakers, J. B. P. H. van der Putten, T. C. T. Geuns, M. Beenhakkers, J. B. Giesbers, B. H. Huisman, E. J. Meijer, E. M. Benito, F. J. Touwslager, A. W. Marsman, B. J. E. van Rens, D. M. de Leeuw, *Nat. Mater.* **2004**, *3*, 106.
- [5] H. Kawaguchi, T. Someya, T. Sekitani, T. Sakurai, *IEEE J. Solid-State Circuits* **2005**, *40*, 177.
- [6] H. Klauk, *Chem. Soc. Rev.* **2010**, *39*, 2643.
- [7] Y. Y. Noh, N. Zhao, M. Caironi, H. Sirringhaus, *Nat. Nanotechnol.* **2007**, *2*, 784.
- [8] U. Pfalinger, C. Auner, H. Gold, A. Haase, J. Kraxner, T. Haber, M. Sezen, W. Grogger, G. Domann, G. Jakopic, J. R. Krenn, B. Stadlober, *Adv. Mater.* **2010**, *22*, 5115.
- [9] T. Yamamoto, K. Takimiya, *J. Am. Chem. Soc.* **2007**, *129*, 2224.
- [10] T. W. Kelley, L. D. Boardman, T. D. Dunbar, D. V. Muyres, M. J. Pellerite, T. P. Smith, *J. Phys. Chem. B* **2003**, *107*, 5877.
- [11] S. Lee, B. Koo, J. Shin, E. Lee, H. Park, H. Kim, *Appl. Phys. Lett.* **2006**, *88*, 162109.
- [12] D. Gundlach, L. Zhou, J. Nichols, T. Jackson, P. Necliudov, M. Shur, *J. Appl. Phys.* **2006**, *100*, 024509.
- [13] A. Benor, D. Knipp, *Org. Electron.* **2008**, *9*, 209.
- [14] V. Wagner, P. Wobkenberg, A. Hoppe, J. Seekamp, *Appl. Phys. Lett.* **2006**, *89*, 243515.
- [15] K. Myny, S. Steudel, S. Smout, P. Vicca, F. Furthner, B. van der Putten, A. Tripathi, G. Gelinck, J. Genoe, W. Dehaene, P. Heremans, *Org. Electron.* **2010**, *11*, 1176.
- [16] M. Kitamura, Y. Arakawa, *Jpn. J. Appl. Phys.* **2011**, *50*, 01BC01.

- [17] C. Shim, F. Maruoka, R. Hattori, *IEEE Trans. Electron Devices* **2010**, *57*, 95.
- [18] S. Wang, Y. Yan, K. Tsukagoshi, *Appl. Phys. Lett.* **2010**, *97*, 063307.
- [19] Y. Yan, X. She, H. Zhu, S. Wang, *Org. Electron.* **2011**, *12*, 823.
- [20] S. Luan, G. Neudeck, *J. Appl. Phys.* **1992**, *72*, 766.
- [21] M. Marinkovic, E. Hashem, K. Chan, A. Gordijn, H. Stiebig, D. Knipp, *Appl. Phys. Lett.* **2010**, *97*, 073502.
- [22] A. D. Franklin, Z. Chen, *Nat. Nanotechnol.* **2010**, *5*, 858.
- [23] J. Smith, Y. Zhao, C. Yang, J. Appenzeller, *68th Annual Device Research Conference (DRC) Technical Digest* **2010**, 139.
- [24] F. Xia, V. Perebeinos, Y. Lin, Y. Wu, P. Avouris, *Nat. Nanotechnol.* **2011**, *6*, 179.
- [25] D. J. Gundlach, T. N. Jackson, D. G. Schlom, S. F. Nelson, *Appl. Phys. Lett.* **1999**, *74*, 3302.
- [26] F. Letzkus, J. Butschke, B. Hoefflinger, M. Irmischer, C. Reuter, R. Springer, A. Ehrmann, J. Mathuni, *Microelectron. Eng.* **2000**, *53*, 609.
- [27] S. Jin, K. Jung, H. Shin, B. Park, J. Lee, *Synth. Met.* **2006**, *156*, 196.
- [28] K. Sidler, N. Cvetkovic, V. Savu, D. Tsamados, A. Ionescu, J. Brugger, *Procedia Chem.* **2009**, *1*, 762.
- [29] F. Fleischli, K. Sidler, M. Schaer, V. Savu, J. Brugger, L. Zuppiroli, *Org. Electron.* **2010**, *12*, 336.
- [30] F. Ante, F. Letzkus, J. Butschke, U. Zschieschang, K. Kern, J. N. Burghartz, H. Klauk, *IEEE International Electron Devices Meeting (IEDM) Technical Digest* **2010**.
- [31] U. Zschieschang, F. Ante, D. Kälblein, T. Yamamoto, K. Takimiya, H. Kuwabara, M. Ikeda, T. Sekitani, T. Someya, J. Blochwitz-Nimoth, H. Klauk, *Org. Electron.* **2011**, *12*, 1370.
- [32] F. Ante, D. Kälblein, U. Zschieschang, T. W. Canzler, A. Werner, K. Takimiya, M. Ikeda, T. Sekitani, T. Someya, H. Klauk, *Small* **2011**, *7*, 1186.
- [33] J. Zaumseil, K. Baldwin, J. Rogers, *J. Appl. Phys.* **2003**, *93*, 6117.
- [34] D. K. Schroder, *Semiconductor Material and Device Characterization*, 2nd ed., Wiley, New York **1998**.
- [35] T. J. Richards, H. Sirringhaus, *J. Appl. Phys.* **2007**, *102*, 094510.
- [36] S. Scheinert, G. Paasch, *J. Appl. Phys.* **2009**, *105*, 014509.
- [37] P. Heremans, J. Genoe, S. Steudel, K. Myny, S. Smout, P. Vicca, C. Grillberger, O. R. Hild, F. Furthner, B. van der Putten, A. K. Tripathi, G. H. Gelinck, *IEEE International Electron Devices Meeting (IEDM) Technical Digest* **2009**.

Received: August 16, 2011

Published online: November 17, 2011